Applied Catalysis B: Environmental 111–112 (2012) 106–118

Contents lists available at SciVerse ScienceDirect

Applied Catalysis B: Environmental

journal homepage: www.elsevier.com/locate/apcatb

$NO/NO_2/N_2O–NH_3$ SCR reactions over a commercial Fe-zeolite catalyst for diesel exhaust aftertreatment: Intrinsic kinetics and monolith converter modelling

Massimo Colombo[a], Isabella Nova[a], Enrico Tronconi[a,*], Volker Schmeißer[b], Brigitte Bandl-Konrad[b], Lisa Zimmermann[c]

[a] Dipartimento di Energia, Laboratorio di Catalisi e Processi Catalitici, Politecnico di Milano, Piazza Leonardo da Vinci 32, I-20133, Milano, Italy
[b] Daimler AG, 019-G206 GR/APE, 70546 Stuttgart, Germany
[c] Daimler AG, 019-D121 TP/PME, 70546 Stuttgart, Germany

ARTICLE INFO

Article history:
Received 7 July 2011
Received in revised form 8 September 2011
Accepted 19 September 2011
Available online 24 September 2011

Keywords:
Urea SCR
Standard SCR
Fast SCR
NO_2 SCR
N_2O decomposition
N_2O reactivity
Zeolite catalysts
Diesel exhaust aftertreatment

ABSTRACT

We present a systematic kinetic investigation of the full $NO/NO_2/N_2O–NH_3$ SCR reacting system performed over a commercial Fe-promoted zeolite catalyst in the form of powder in a representative temperature range (150–550 °C) at high space velocities. The well-known reactions of the $NO/NO_2–NH_3$ SCR system, namely NH_3 adsorption, NH_3 and NO oxidation, standard-, fast- and NO_2-SCR reactions, ammonium nitrate formation, and N_2O formation are considered. In addition, dedicated runs with N_2O added to the feed stream showed that two more reactions, namely N_2O reduction by NO ($N_2O + NO \rightarrow N_2 + NO_2$) and N_2O reduction by NH_3 ($2NH_3 + 3N_2O \rightarrow 4N_2 + 3H_2O$) become significant at $T > 330$ °C and need to be considered for kinetic modelling.

The kinetic runs were fitted by multiresponse nonlinear regression to obtain estimates of the intrinsic rate parameters. Such parameters, as well as the relevant geometrical and morphological catalyst properties, were then successfully used to simulate on a purely predictive basis additional transient SCR runs performed over core honeycomb samples of the same Fe-zeolite catalyst, revealing modest effects of mass transfer limitations.

In comparison with other published SCR kinetic models, the model herein developed accounts also for the N_2O reactivity with NO and NH_3, which is shown to be an important feature in order to accurately reproduce high-T operation of SCR converters based on Fe-zeolite catalysts.

1. Introduction

Nowadays, one of the challenges in the development of diesel vehicles is the limitation of pollutants emission in order to fulfil new government regulations, especially in relation to NO*x* and particulate matter (PM) [1]. Focusing on NO*x*, the more and more restrictive legislations have driven the development of new aftertreatment technologies, among which NH_3/urea SCR (selective catalytic reduction) is considered one of the most effective [1]. During the last decade such a technology, already extensively applied in the past to the abatement of NO*x* emitted from stationary sources [2,3], has been adapted to mobile applications. To succeed in this technology transfer, a big effort has been first devoted to study the Standard SCR reaction, in which NH_3 is used to reduce mainly NO present in the exhausts ($2NH_3 + 2NO + 1/2O_2 \rightarrow 2N_2 + 3H_2O$). More recently, the other reactions occurring when the concentration of NO_2 in the exhausts is significant have been analyzed in details, too [2,4–6]. Indeed, onboard of vehicles the SCR converter is usually integrated in a complex aftertreatment system where a diesel oxidation catalyst, and sometimes a catalyzed diesel particulate filter, as well are placed upstream of the SCR unit, leading to the partial conversion of NO to NO_2. This greatly enhances the DeNO*x* efficiency as the Fast SCR reaction, which involves the reaction of NH_3 with an equimolar mixture of NO and NO_2 ($2NH_3 + NO + NO_2 \rightarrow 2N_2 + 3H_2O$) [2,4,6–11], becomes active. Furthermore, in the presence of excess NO_2, also the "NO_2" SCR reaction ($8NH_3 + 6NO_2 \rightarrow 7N_2 + 12H_2O$) [2,4,5,7,9] can significantly contribute to the overall DeNO*x* activity. To complete the picture, we also need to consider N_2O: this species may be an undesired by-product of the SCR reactions formed in small amounts under certain conditions, but can also either decompose or be reduced by NH_3 to N_2 over Fe-zeolite catalysts. Nevertheless, this reactivity has been so far neglected in the studies addressing the SCR DeNO*x* kinetics over such systems.

As mentioned above, SCR converters are usually integrated in complex aftertratment systems whose design and optimization is often a challenging and expensive task. In this context, the development of modelling tools is a key factor in order to reduce costs and time associated with commercialization.

* Corresponding author. Tel.: +39 02 2399 3264; fax: +39 02 2399 3318.
E-mail address: enrico.tronconi@polimi.it (E. Tronconi).

0926-3373/$ – see front matter © 2011 Elsevier B.V. All rights reserved.
doi:10.1016/j.apcatb.2011.09.023

Nomenclature

C_i	gas-phase concentration of species i (mol/m^{3}gas)
E_j	rate parameter for T-dependence of reaction j (K)
k^o_j	logarithm of rate constant of reaction j at T_{ref} (–)
k_{ads}	rate constant for NH_3 adsorption (m^3/mol/s)
K_{NO_2}	rate parameter in Eq. (5) (–)
$K^{eq}_{NO_2}$	equilibrium constant of reaction (R.4) (1/bar$^{0.5}$)
P_{O_2}	partial pressure of O_2 (bar)
Q	flow rate (cm^3/min)
R	ideal gas constant (J/mol K)
r_j	rate of reaction j (mol/m^3/s)
T	temperature (K)
T_{ref}	reference temperature (K)
α	parameter for surface coverage dependence, Eq. (2) (–)
γ	rate parameter in Eq. (3) (–)
ε	rate parameter in Eq. (14) (mol/m^3)
θ_{NH_3}	NH_3 surface coverage on S2 sites (–)
ϑ_{Nit}	NH_4NO_3 surface coverage on S2 sites (–)
σ	NH_3 surface coverage on S1 sites (–)

Within this framework, the present work was aimed at investigating a commercial, state-of-the-art Fe-promoted zeolite catalyst in all the $NO/NO_2/N_2O$–NH_3 SCR reactions. Catalytic activity runs were performed in a representative temperature range (150–550 °C) at high space velocities (GHSV ≥100,000 h^{-1}) over the catalyst in the form of powder in order to gain intrinsic kinetic information on the complete SCR reaction network, including N_2O-related reactions. Such parameters, as well as the relevant geometrical and morphological catalyst properties, were then incorporated in a dedicated 1D + 1D mathematical model of SCR monolithic converters to simulate successfully transient SCR runs performed over core honeycomb samples of the same catalyst.

To our knowledge, this is the first SCR kinetic model accounting for the N_2O reactivity as well, thus providing a full description of the NH_3-SCR reacting system.

2. Methods

A commercial Fe-zeolite SCR catalyst was studied following the same stepwise scale-up approach already used in the past in our labs for vanadium-based and other metal-promoted zeolite SCR catalysts [12–14]. The work started from the study of the catalyst in the form of crushed monolith powder, in order to gain intrinsic kinetic information. At a second stage, lab-scale experiments were performed on small honeycomb monolith samples in a different lab rig, in order to comparatively evaluate the importance of transport phenomena. Within the following subsections the adopted experimental procedures are described in more detail.

2.1. Lab scale experiments

Kinetic runs were carried out over the catalyst in the form of powder (80 mg), obtained by grinding and sieving (140–200 mesh) the original commercial Fe-zeolite washcoated monolith catalyst. The catalyst powder was loaded in a flow-microreactor consisting of a quartz tube (6 mm i.d.) placed into an electric furnace with a thermocouple directly immersed in the catalyst bed to measure the reaction temperature. The reactor was directly connected to a quadrupole mass spectrometer (Balzers QMS 200), for analysis of N_2O and N_2 and to a UV-analyzer (ABB LIMAS 11HW), for analysis of NO, NO_2 and NH_3 in parallel. NH_3, NO, NO_2, N_2O, O_2 and He were dosed from bottled calibrated gas mixtures by mass flow controllers, while water vapor was added by means of a saturator.

The catalyst was conditioned in a T-ramp at 5 °C/min up to 600 °C in 8% O_2 v/v, and 8% H_2O v/v and keeping it at 600 °C for 5 h. Kinetic runs included both isothermal steady-state experiments and temperature programmed reaction (TPR) experiments performed within the 150–550 °C temperature range; in the case of the TPR runs the heating rate was 2 °C/min. Furthermore, reaction dynamics were investigated by isothermal step response runs, i.e. feeding in a stepwise manner one of the reactants while continuously flowing the other species, within the 200–300 °C T-range. Typical feed concentrations of NOx (with $0 \le NO_2/NOx \le 1$), N_2O and NH_3 were 500 or 1000 ppm, always in the presence of O_2 (8% v/v) and H_2O (8% v/v) and balance He. The system was operated at atmospheric pressure with a Gas Hourly Space Velocity (GHSV) in the range 205,000–682,000 cm^3/min g_{cat} (STP). A detailed description of the experimental equipment and procedures can be found in [13–16].

The NH_3-SCR reactions were also investigated over core drilled monolith samples (volume ≅6 cm^3, cell density = 400 c psi, wall thickness = 5 mils and mean washcoat thickness around 0.080 mm) under isothermal steady-state and transient conditions within the 150–550 °C T-range. The catalyst conditioning procedure was the same as for the powder samples. Typical feed concentrations of NOx, N_2O and NH_3 were 200–500 ppm, with O_2 = 8% v/v and H_2O = 8% v/v and balance N_2. The space velocity, in this case referred to the monolith volume, was set to 100,000 h^{-1}.Outlet gases were analyzed using a UV-analyzer (ABB LIMAS 11HW) for NO, NO_2, NH_3 and a Non Dispersive IR Analyzer (ABB URAS-14) for N_2O.

2.2. Model

2.2.1. Reaction network and kinetics

For the purposes of the present work we have developed a global dual-site kinetic model of the $NO/NO_2/N_2O$–NH_3 SCR reacting system. Such a model is based on previous ones developed for vanadia catalysts [13,16,17] and for a Fe-zeolite catalyst [12], but it has been herein extended to include also the SCR reactivity in presence of excess NO_2 and particularly to describe the reactivity of N_2O, too. In the following we report the reactions included in the kinetic model, and the corresponding rate equations.

To describe the NH_3 adsorption–desorption processes, in line with previous proposals for V-based catalysts [15,18], Eq. (1) assumes a non-activated NH_3adsorption onto the acidic catalyst sites S2 (herein represented by *), while for the NH_3 desorption process Eq. (2) takes into account the heterogeneity of the catalyst surface, associated with a range of desorption activation energies.

NH_3 adsorption/desorption onto S2 (*) sites

$$NH_3 \Leftrightarrow NH_3* \quad \text{(R.1)}$$

$$r_{ads} = k_{ads} C_{NH_3}(1 - \theta_{NH_3} - \vartheta_{Nit}) \quad (1)$$

$$r_{des} = \exp[k^o_{des} - E_{des}\left(\frac{1000}{T}(1 - \alpha\theta_{NH_3}) - \frac{1000}{473}\right)]\theta_{NH_3} \quad (2)$$

Two different reactions have been considered for NH_3 oxidation, leading to different products, namely N_2 and NO ((R.2) and (R.3), respectively). In line with experimental evidence presented below (see paragraph on "Steady state and transient NH_3/NO–NO_2/O_2 catalytic activity"), a promoting effect of NO on the NH_3 oxidation to N_2 was also empirically included in (Eq. (3)): this term is also further discussed in the following. Regarding NO oxidation, reaction (R.4) is reversible, limited by thermodynamic constraints, and inhibited by NO_2, see (Eq. (5)).

NH_3 oxidation to N_2

$$NH_3* + 3/4O_2 \rightarrow 1/2N_2 + 3/2H_2O \quad \text{(R.2)}$$

$$r_{ox} = \exp\left(k^o_{ox} - E_{ox}\left(\frac{1000}{T} - \frac{1000}{473}\right)\right)\theta_{NH_3}(1+\gamma\cdot C_{NO}) \quad (3)$$

NH_3 oxidation to NO

$$NH_3* + 5/4O_2 \rightarrow NO + 3/2H_2O \quad (R.3)$$

$$r_{oxb} = \exp\left(k^o_{oxb} - E_{oxb}\left(\frac{1000}{T} - \frac{1000}{473}\right)\right)\theta_{NH_3} \quad (4)$$

NO oxidation to NO_2

$$NO + 1/2O_2 \leftrightarrow NO_2 \quad (R.4)$$

$$r_{NO_{ox}} = \exp\left(k^o_{NO_{ox}} - E_{NO_{ox}}\left(\frac{1000}{T} - \frac{1000}{473}\right)\right) \times \frac{(C_{NO}\sqrt{P_{O_2}} - (C_{NO_2}/K^{eq}_{NO_2}))}{1 + K_{NO_2}C_{NO_2}} \quad (5)$$

In the case of the Standard SCR reaction (R.5), a dual-site Mars-Van Krevelen rate expression assuming that NH_3 may block the red-ox sites for NO activation (S1 sites) was adopted in our previous work for both vanadium based [14,16] and Fe-zeolite catalysts [12] in order to explain the observed inhibiting effect of NH_3 on such a reaction at low temperatures. Based on similar experimental evidence and thus on similar assumptions, a consistent but simplified rate expression for the Standard SCR reaction, (Eq. (6)) + (Eq. (7)), has been derived in this work to describe the rate of the Standard SCR reaction (R.5). Notably, in previous work a spillover step of NH_3 from adsorption (S2) to reaction (S1) sites had been assumed, while a direct inhibition of NH_3 via adsorption/desorption onto the red-ox sites S1 (R.6) has been implemented herein. In Eqs. (6) and (7), $(1-\sigma_{NH_3})$ represents in fact the fraction of available S1 red-ox sites, whereas σ_{NH_3} is the fraction of S1 red-ox sites blocked by NH_3.

Standard SCR (Low T)

$$NH_3* + NO + 1/4O_2 \rightarrow N_2 + 3/2H_2O \quad (R.5)$$

$$r_{NO} = \exp\left(k^o_{Std} - E_{NO}\left(\frac{1000}{T} - \frac{1000}{473}\right)\right) C_{NO}\theta_{NH_3}(1-\sigma_{NH_3}) \quad (6)$$

Adsorption/desorption of inhibiting NH_3 onto S1 red-ox sites

$$S_1 + NH_3 \Leftrightarrow S_1[NH_3] \quad (R.6)$$

$$r_{Ads/Des\text{-}S1} = \exp\left(k^o_{Ads\text{-}S1} - E_{Ads\text{-}S1}\left(\frac{1000}{T} - \frac{1000}{473}\right)\right) \times C_{NH_3}(1-\sigma_{NH_3}) - \exp\left(k^o_{Des\text{-}S1} - E_{Des\text{-}S1}\left(\frac{1000}{T} - \frac{1000}{473}\right)\right)\sigma_{NH_3} \quad (7)$$

A kinetic description of buildup-depletion of NH_3 onto the S1 active sites, as implemented in Eq. (7), was found necessary in order to reproduce the observed transient features associated with NH_3 inhibition effects, e.g. the hysteresis cycles discussed below.

In order to fully account also for the observed NH_3/NO reactivity at temperatures higher than 500 °C, where the NH_3 desorption kinetics lead to negligibly low NH_3 coverages, a second Standard SCR reaction (R.7) was also included in the reaction network, with a rate expression depending only on the gas-phase reactants concentrations, as proposed by Sjövall et al. [19] for a Fe-zeolite catalyst.

Standard SCR (High T)

$$NH_3 + NO + 1/4O_2 \rightarrow N_2 + 3/2H_2O \quad (R.7)$$

$$r_L = \exp\left[k^o_L - E_L\left(\frac{1000}{T} - \frac{1000}{823}\right)\right] C_{NO}C_{NH_3} \quad (8)$$

The possible presence of large amounts of NO_2 in a wide range of temperatures requires the implementation of additional reactions, (R.8)–(R.12), namely ammonium nitrate formation/dissociation, N_2O formation, NO_2-SCR and fast SCR. "Ammonium nitrate" adsorbed species were assumed to form onto the same S2 sites where NH_3 is adsorbed. In the following rate expressions, σ_{Nit} is the fractional surface coverage of "ammonium nitrate" adsorbed species.

Ammonium nitrate build-up

$$2NO_2 + 2NH_3* \rightarrow NH_4NO_3* + N_2 + H_2O \quad (R.8)$$

$$r_{Amm} = \frac{\exp(k^o_{Amm} - E_{Amm}((1000/T) - (1000/473)))\theta_{NH_3}C^2_{NO_2}}{1 + K_{amm}\vartheta_{Nit}} \quad (9)$$

Ammonium nitrate dissociation/sublimation

$$NH_4NO_3* \rightarrow (NH_3 + HNO_3) \rightarrow NH_4NO_3(s) \quad (R.9)$$

$$r_{Nit} = \exp\left(k^o_{Nit} - E_{Nit}\left(\frac{1000}{T} - \frac{1000}{473}\right)\right)\vartheta_{Nit} \quad (10)$$

N_2O formation

$$2NH_3* + 2NO_2 \rightarrow N_2O + N_2 + 3H_2O \quad (R.10)$$

$$r_{N_2O} = \exp\left(k^o_{N_2O} - E_{N_2O}\left(\frac{1000}{T} - \frac{1000}{473}\right)\right)\theta_{NH_3}C_{NO_2} \quad (11)$$

NO_2-SCR

$$NH_3* + 3/4NO_2 \rightarrow 7/8\,N_2 + 3/2H_2O \quad (R.11)$$

$$r_{NO_2} = \exp\left(k^o_{NO_2} - E_{NO_2}\left(\frac{1000}{T} - \frac{1000}{473}\right)\right)\theta_{NH_3}C_{NO_2} \quad (12)$$

Fast SCR

$$2NH_3* + NO + NO_2 \rightarrow 2N_2 + 3H_2O \quad (R.12)$$

$$r_{Fast} = \exp\left(k^o_{Fast} - E_{Fast}\left(\frac{1000}{T} - \frac{1000}{473}\right)\right)\theta_{NH_3}C_{NO_2}C_{NO} \quad (13)$$

Finally, two more reactions were included in order to describe the N_2O reactivity on Fe-zeolite under typical NH_3-SCR conditions, namely the N_2O reduction by NO [20–22] (R.13) and the selective reduction of N_2O by NH_3 to N_2 [23,24] (R.14).

N_2O reduction by NO

$$N_2O + NO \rightarrow N_2 + NO_2 \quad (R.13)$$

$$r_{N_2O\ DC} = \exp\left(k^o_{N_2O\,DC} - E_{N_2O\,DC}\left(\frac{1000}{T} - \frac{1000}{473}\right)\right) \times C_{N_2O}\left(\frac{C_{NO}}{C_{NO} + \varepsilon}\right) \quad (14)$$

N_2O-SCR with NH_3

$$NH_3* + 3/2\,N_2O \rightarrow 2\,N_2 + 3/2H_2O \quad (R.14)$$

$$r_{N_2O\,R} = \exp\left(k^o_{N_2O\,R} - E_{N_2O\,R}\left(\frac{1000}{T} - \frac{1000}{473}\right)\right)\theta_{NH_3}C_{N_2O} \quad (15)$$

Notice that the combination of reactions (R.13) and ((R.4) reverse) results in the stoichiometry of the direct N_2O decomposition:

$$N_2O \rightarrow N_2 + 1/2O_2 \quad (R.15)$$

The reaction scheme herein proposed, however, is in line with the "catalytic" nature of the NO promotion of N_2O decomposition, well established in the literature and reported for various Fe-zeolites [20–22]. In fact, it predicts that N_2O decomposition can be activated even by just small traces of NO. Again in agreement with such a "catalytic" effect [25], we have adopted zero-order

kinetics in NO for reaction (R.13): in (Eq. (14)), in fact, the rate parameter ε is a very small number ($\cong 10^{-3}$), so that the rate of the N_2O reaction with NO is virtually independent of the NO concentration, but when such a concentration becomes negligible.

It is worth mentioning also that the inclusion of reactions (R.13) and (R.14) in the SCR kinetic model allows in principle to account for the effect of NO addition on the NH_3-SCR of N_2O observed by Guzmán-Vargas et al. [20]. In the cited reference the authors reported that, over selected Fe-zeolite catalysts, N_2O reduction by NH_3 was promoted by the presence of NO, and explained the possible promoting effect of NO on N_2O reduction by the analysis of the reaction rates in the following mechanistic scheme:

$$N_2O + * \rightarrow N_2 + O* \quad \text{(R.16)}$$

$$3O* + 2NH3 \rightarrow N2 + 3H_2O + 3* \quad \text{(R.17)}$$

$$NO + O* \rightarrow NO_2* \quad \text{(R.18)}$$

Reactions (R.17) and (R.18) are regarded by Guzmán-Vargas et al. [20] as the rate determining steps of N_2O reduction by NH_3 and by NO, respectively. When reaction (R.17) is faster than (R.18), no promoting effect of NO on the SCR of N_2O is expected, while a promoting effect becomes apparent in the opposite case. In the model herein proposed the two considered global reactions of N_2O, namely the SCR of N_2O by NH_3 (R.14) and the N_2O reduction by NO (R.13) are indeed equivalent to the above scheme of Guzmán-Vargas et al. Since we estimated the rate parameters of both reactions independently from dedicated tests, our model describes the possible promoting effect of NO as a simple superposition of the N_2O reactivity with NO and with NH_3.

The parameters of the rate expressions (Eqs. (1)–(15)) for reactions ((R.1)–(R.14)) were estimated by multi response nonlinear regression of the transient microreactor runs, as detailed below. Notice that the rate equations do not include dependences on O_2 and H_2O, since the feed concentrations of both such species were kept constant at 8% v/v.

2.2.2. Monolith SCR converter model

The model of the honeycomb monolith SCR catalyst is similar to that already reported in [12–14], but for the inclusion of the additional reactions. Briefly, the heterogeneous dynamic 1D + 1D model of a single monolith channel in this case includes the unsteady differential mass balance equations of five gaseous species (NH_3, NO, NO_2, N_2, N_2O) and of three adsorbed species (NH_3*, S1 [NH_3], NH_4NO_3*). Enthalpy balances for the gas and for the solid phase are included to account also for thermal effects. In addition, external (gas–solid) mass transfer is described by means of well established correlations for mass transfer coefficients, while intra-phase diffusional limitations are accounted for by equations for diffusion-reaction of the gaseous reactants in the porous catalytic washcoat, using species effective diffusivities of the order of 10^{-7} m^2/s at 200 °C [26,27].

3. Results and discussion

3.1. Kinetic runsover powdered catalyst

3.1.1. NH_3 adsorption–desorption

The interaction of NH_3 with the catalyst surface is obviously important for SCR applications, as it is well known that the DeNO*x* performances and the dynamics of SCR converters are governed by the reactivity of adsorbed NH_3.The adsorption–desorption behaviour of NH_3 was first studied performing a two-stages run, namely an isothermal NH_3feed concentration step change (TRM) followed by a Temperature Programmed Desorption (TPD) experiment.

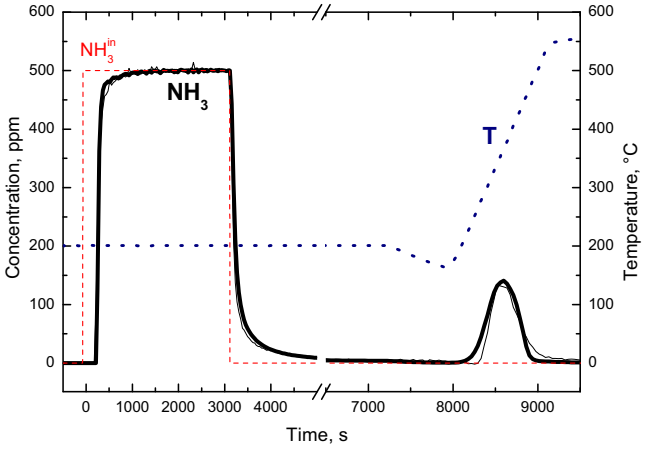

Fig. 1. Ammonia adsorption and TPD over crushed monolith powder: T = 200 °C, Q = 75 cm^3/min (STP), NH_3 = 500 ppm, H_2O = 8% v/v, O_2 = 0%, T-ramp = 20 °C/min. Thin line = experimental. Thick line = kinetic fit.

The thin line in Fig. 1 shows the NH_3 concentration trace measured at the reactor outlet during the complete adsorption/desorption + TPD test. First, at t = 0 s, a step feed change (0–500 ppm) of the NH_3 inlet concentration at a constant temperature of 200 °C was performed while flowing H_2O (8% v/v) and balance helium through the reactor. This resulted first in a dead time in the NH_3 outlet concentration, followed by its slow increase with time, until a steady state concentration equal to the feed value was reached. This transient behaviour is attributed to the adsorption of NH_3 onto the catalyst [4], as NH_3 oxidation can be surely ruled out due to the absence of O_2.

After catalyst saturation, at t = 3000 s NH_3 was removed from the feed flow, and afterwards the catalyst was continuously flushed at constant temperature with helium and H_2O for about 1 h. During this period of time (3000 < t < 8000 s) a broad desorption tail was observed, likely due to the desorption of weakly adsorbed NH_3.

The adsorption/desorption test continued with a linear increase of the temperature at 20 °C/min up to 550 °C (TPD run). Before starting the temperature ramp the catalyst was cooled down to about 150 °C, in order to have an effective linear increase of the temperature above 200 °C. As the temperature exceeded 200 °C ($t \approx 8100$ s), a desorption peak in the NH_3 outlet concentration was observed, due to the release of the previously strongly adsorbed NH_3 species. The peak reached the maximum concentration close to 150 ppm slightly above 350 °C, and then decreased until all the previously adsorbed NH_3 was totally desorbed.

The same experiment was then replicated changing either the NH_3 feed concentration (from 500 to 1000 ppm), or the adsorption temperature (from 200 to 150 °C) of the adsorption/desorption phase, or the heating rate (from 20 to 15 °C/min) of the TPD run. The results, herein not reported for brevity, were in line with the experiment shown in Fig. 1 and were then used for kinetic fitting purposes. Indeed, the whole set of experimental results was analyzed according to a dynamic one-dimensional isothermal heterogeneous plug-flow model of the test microreactor, as described in [15,16]. A global nonlinear regression provided the estimates of the rate parameters for the NH_3 adsorption/desorption reaction (R1) included in the kinetic model. The coverage-dependent desorption energy was found in line with previous literature reports on zeolites [28,29], with an order of magnitude in excess of 100 kJ/mol at zero NH_3 coverage.

The solid thick line in Fig. 1 represents the kinetic fit of the run described above. The model is able to predict with a satisfactory degree of accuracy both the NH_3 adsorption and desorption behaviours. Indeed, there is a good match between predicted and observed NH_3 dead time, NH_3 closure dynamics and TPD curve.

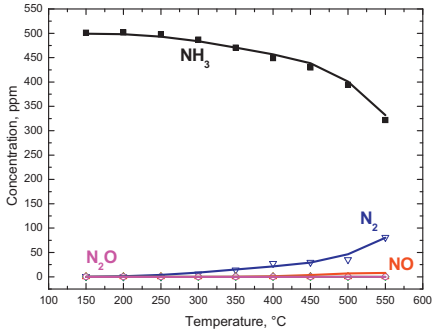

Fig. 2. Reactivity of NH_3–O_2 as a function of temperature over crushed monolith powder: Q = 250 cm³/min (STP), NH_3 = 500 ppm, H_2O = 8% v/v, O_2 = 8% v/v. Symbols = experimental. Solid lines = kinetic fit.

A similar agreement between experimental and calculated results was obtained for all the experiments included in the model fit.

3.1.2. Steady state NH_3/O_2, NO/O_2, NO_2/O_2 catalytic activity

To investigate the catalyst activity in the NH_3 oxidation (R.2)–(R.3) and in the reversible NO oxidation reaction (R.4), steady state runs were performed in the 150–550 °C T-range feeding to the reactor 500 ppm of either NH_3, NO or NO_2 together with O_2 (8% v/v), H_2O (8% v/v) and balance helium. NH_3 started to be significantly oxidized at temperatures greater than 300 °C (see Fig. 2 symbols), giving N_2 as the main product. Traces of NO were also detected above 450 °C, motivating the introduction of (R.3) and Eq. (4) in the kinetic model.

Fig. 3 (symbols) shows that NO oxidation reached a maximum of 10% NO conversion around 450 °C, while at higher temperatures thermodynamic equilibrium was approached. Finally, the inverse of NO oxidation, namely NO_2 decomposition to NO, was found to become significant at temperatures greater than 350 °C, as shown in Fig. 4 (symbols).

A global multi response nonlinear regression on this data set provided the estimates of the rate parameters for reactions (R.2)–(R.4) (see solid lines in Figs. 2–4).

3.1.3. Steady state and transient NH_3/NO–NO_2/O_2 catalytic activity

The NH_3/NO–NO_2/O_2 SCR reactivity was then studied over the powdered catalyst. The focus of the study was to investigate the

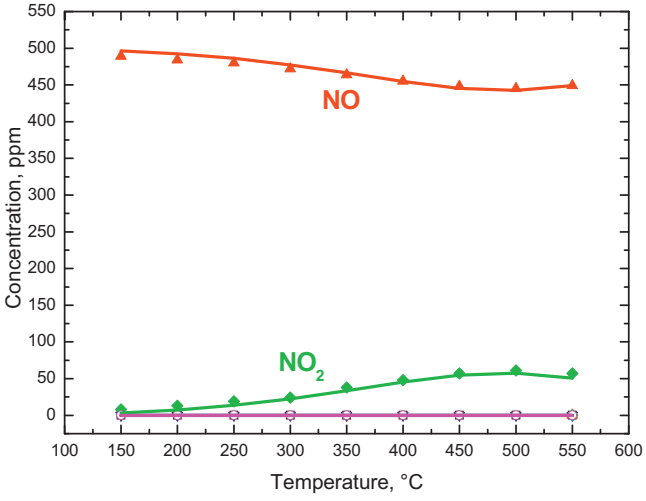

Fig. 3. Reactivity of NO–O_2 as a function of temperature over crushed monolith powder: Q = 250 cm³/min (STP), NO = 500 ppm, H_2O = 8% v/v, O_2 = 8% v/v. Symbols = experimental. Solid lines = kinetic fit.

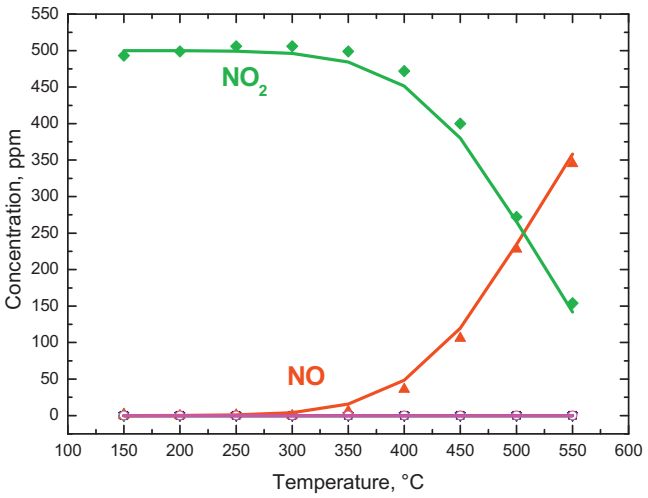

Fig. 4. Reactivity of NO_2–O_2 as a function of temperature over crushed monolith powder: Q = 250 cm³/min (STP), NO_2 = 500 ppm, H_2O = 8% v/v, O_2 = 8% v/v. Symbols = experimental. Solid lines = kinetic fit.

effect of the NO_2/NOx feed ratio on the DeNOx activity, covering the whole $0 \leq NO_2/NOx \leq 1$ range in the wide temperature window of practical interest (150–550 °C).

In Fig. 5 thin lines show the experimental results obtained during a slow temperature ramp (2 °C/min) from 150 °C up to 550 °C when continuously feeding to the reactor 500 ppm of both NH_3 and NO while flowing O_2 (8% v/v), H_2O (8% v/v) and balance helium. Such a slow temperature ramp allows the catalyst to approach pseudo-steady state conditions in the whole T-range: this was verified by comparing the NO conversions measured during the temperature ramp with results collected during isothermal steady state runs (see for example, steady state data in Fig. 6A).

As evident in Fig. 5, in the whole investigated temperature range a growing consumption of NH_3 and NO, with corresponding evolution of N_2, was observed with increasing temperature. The outlet species concentrations were initially consistent with the stoichiometry of the Standard SCR reaction (R.5) and pointed out 100% selectivity to N_2. However, above 250 °C a greater consumption of NH_3 with respect to NO was also observed, likely due to the onset of a significant NH_3 oxidation activity [19,30,31]. Regarding this last aspect, it is worth emphasizing that in the absence of NO the threshold temperature for NH_3 oxidation, observed in dedicated

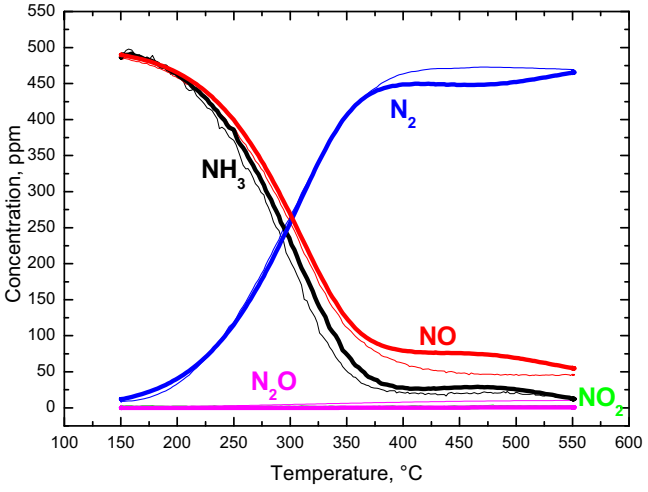

Fig. 5. TPR of NH_3–NO–O_2 over crushed monolith powder: Q = 250 cm³/min (STP), NH_3 = 500 ppm, NO = 500 ppm, H_2O = 8% v/v, O_2 = 8% v/v. T-ramp = 2 °C/min. Thin lines = experimental. Thick lines = kinetic fit.

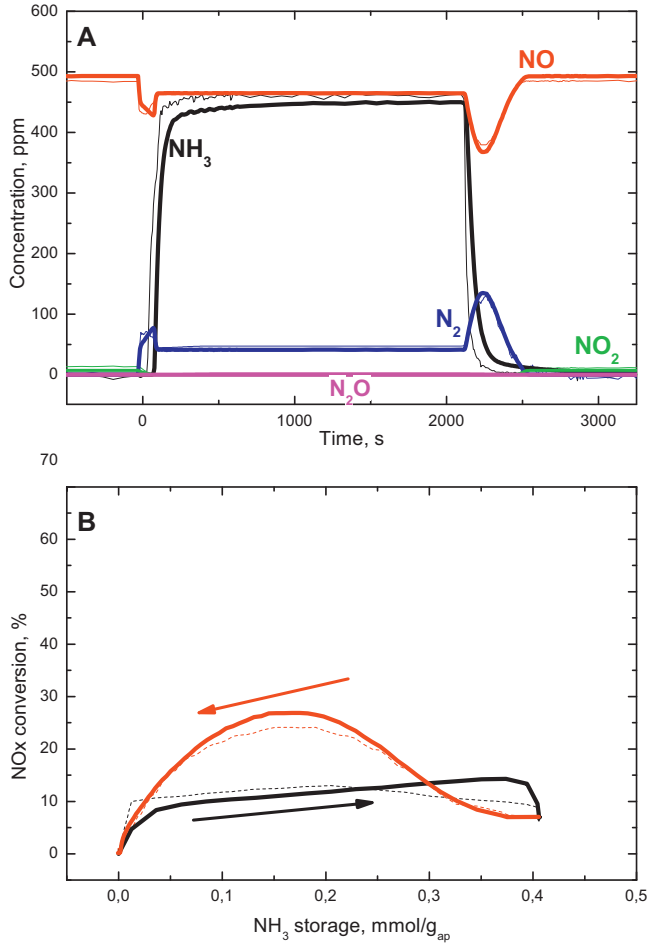

Fig. 6. (A) Concentration step change experiment for the NH_3–NO–O_2 reacting system over crushed monolith powder: T = 200 °C, Q = 250 cm^3/min (STP), NH_3 = 500 ppm, NO = 500 ppm, H_2O = 8% v/v, O_2 = 8% v/v. Thin lines = experimental. Thick lines = kinetic fit. (B) Coverage dependence of NO*x* conversion during the transient experiment of Fig. 6(A). Dashed lines: measured NO*x* conversion. Thick lines: kinetic fit. Black lines = NO*x* conversion during ammonia feed; Red lines = NO*x* conversion during ammonia shut-off. (For interpretation of the references to color in this figure legend, the reader is referred to the web version of the article.)

tests described in the previous paragraph, was around 300 °C, i.e. at least 50 °C higher than the threshold temperature observed in the presence of NO. In order to account for such experimental differences, a promoting effect of NO on the NH_3 oxidation to N_2 was empirically included in the related rate expression (Eq. (3)). One could speculate that the co-presence of NO and O_2 in the feed stream would result in the formation of highly oxidized NO*x* species on the catalyst surface, whose reduction would then require over stoichiometric amounts of NH_3. The related mechanistic implications will be addressed in future work.

Some feed step change (TRM) runs were then performed between 200 and 300 °C to study the dynamic behaviour of the Fe-zeolite catalyst in the Standard SCR reaction. In each run 500 ppm of NH_3 were fed to the reactor in a stepwise manner while continuously flowing NO (500 ppm), O_2 (8% v/v), H_2O (8% v/v) and balance helium. The outlet concentration profiles of NH_3, NO, N_2 and N_2O during a run at 200 °C are plotted versus time in Fig. 6A (thin lines). The NH_3 outlet concentration trace exhibited a dead time and then rapidly grew, eventually approaching a steady-state level of about 460 ppm. At the same time, the NO signal rapidly dropped to a minimum, after which it rose up approaching about 460 ppm at steady state. At NH_3 shut-off a maximum in the DeNO*x* activity was also apparent, while the NH_3 concentration rapidly dropped to zero. The N_2 signal mirrored that of NO, exhibiting identical transient effects with simultaneous N_2 peaks at both NH_3 feed and shut-off. At steady state, the concentrations of NO, NH_3 and N_2 were consistent with the stoichiometry of the Standard SCR reaction (R.5).

Similar dynamic behaviours have been already reported on several Fe zeolites [9,19,32] as well as over vanadium based SCR catalysts [16] and on H-ZSM-5 zeolites [33,34]. It was proposed that the increase in the DeNO*x* activity observed at NH_3 opening and shut-off could be associated with an inhibiting effect of NH_3 on the Standard SCR reaction [16] due to NH_3 blocking the catalyst redox sites, preventing their reoxidation by O_2 and/or the activation of NO. A negative effect is thus played by the excess NH_3 present on the catalyst surface or in the gas phase, which suggests the existence of an optimum value for the NH_3 surface concentration. Adsorption of NH_3 on Fe sites, inhibiting the Standard SCR activity over Fe-zeolites, was also reported by FTIR study in [35].

Such dynamic effects related to NH_3 inhibition are important in practical applications as well, as they can guarantee enhanced DeNO*x* conversions during transient operation of the SCR systems and are thus crucial in the development of NH_3 dosing strategies. Accordingly, in order to better understand the NH_3-coverage dependence of the NO*x* conversion, in Fig. 6B we have replotted the evolution of the NO conversion as a function of the NH_3 surface concentration during the NH_3 feed and shut-off transients of the same TRM run presented above (dashed lines). The surface concentration of NH_3 was calculated from the integral difference between inlet and outlet NH_3concentrations, taking into account that a part of the NH_3 fed to the reactor was converted to N_2 according to the stoichiometry of the STD-SCR reaction, and that the over consumption of NH_3 with respect to NO at steady state was attributed to the NH_3 oxidation reaction. During the NH_3 feed transient (dashed black line in Fig. 6B) the NO conversion initially increased with growing NH_3 coverage, reaching about 13% for a NH_3 surface concentration of 0.2 mmol/$g_{a.p.}$ (mmol per gram of catalytic active phase). Then, for higher NH_3 surface coverages, the NO conversion started to drop, reaching 7% at steady state, when the NH_3 surface concentration was maximum. During the NH_3 shut-off transient (dashed red line in Fig. 6B) the NO conversion was still coverage dependent, exhibiting again a maximum. However, in this case the maximum NO conversion was about 24% for an NH_3 surface concentration of about 0.17 mmol/$g_{a.p.}$, pointing out that quite a different NO*x* conversion can be associated with the same NH_3 surface coverage during these transient phases, resulting in hysteresis cycles. Recently, Kamasamudram et al. [30] reported a similar coverage dependence of NO*x* conversions during NH_3 feed and shut-off transients over a Fe-zeolite SCR catalyst. The authors observed higher NO*x* conversions during the NH_3 feed transients, and explained it by speculating that the presence of NH_3 in the gas phase leads to a higher coverage of the active sites and thus to a higher reaction rate. However, this explanation is in contrast with the results in Fig. 6B, where the maximum DeNO*x* activity was observed during the NH_3 shut-off transient. Other results of ours, not reported for brevity, confirm that the maximum DeNO*x* activity may be actually observed during either the NH_3 feed or the NH_3 shut-off transients, depending on the operating conditions, and cannot therefore be uniquely correlated with the evolution of the gaseous NH_3 concentration.

The same transient tests were performed also at higher temperatures, namely 225, 250, 275 and 300 °C: the dynamics observed at both NH_3 feed and shut-off became less pronounced as the temperature was increased. In parallel, higher temperatures positively affected the steady-state NO*x* conversion, which grew from 8% at 200 °C up to 40% at 300 °C, in line with TPR data in Fig. 5.

Keeping a constant feed concentration of 500 ppm of total NO*x*, 500 ppm of NH_3, O_2 (8% v/v), H_2O (8% v/v) and balance helium, steady state activity data were collected in the 150–550 °C T-range changing the NO_2/NO*x* feed ratios from 0 (data in Figs. 5 and 6) up

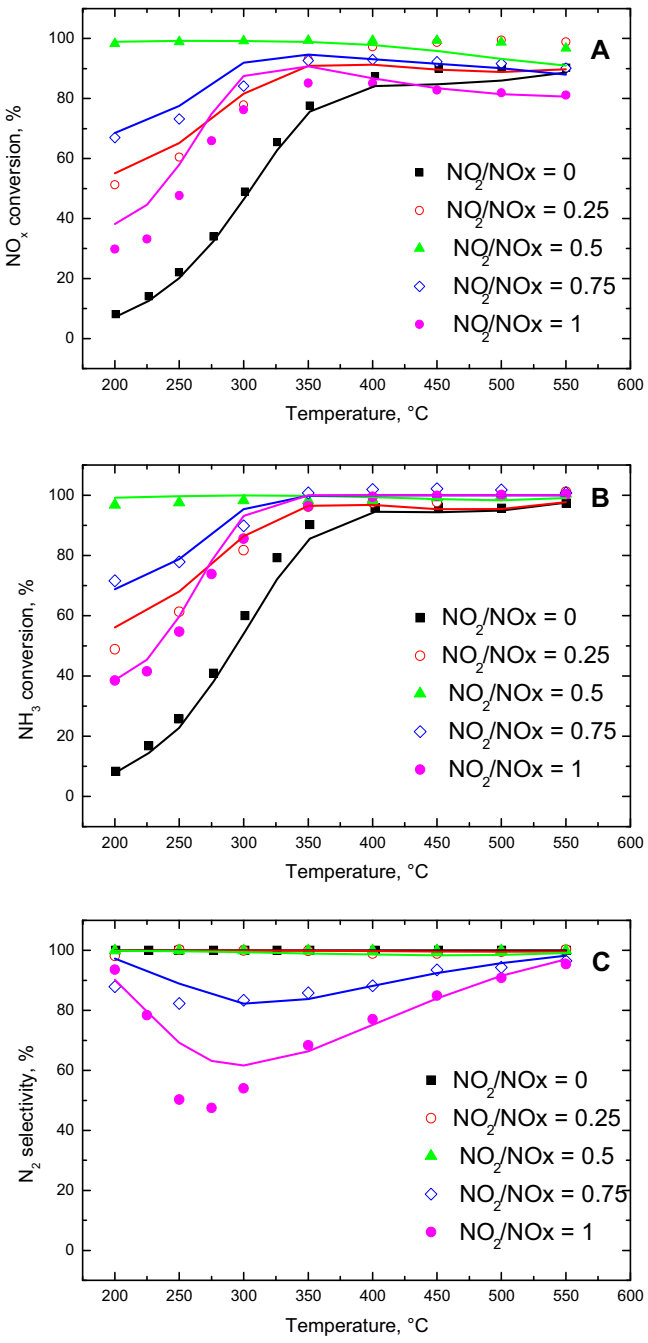

Fig. 7. Effect of the NO_2/NOx feed ratio on the steady-state SCR activity over crushed monolith powder. $Q = 250\ cm^3/min$ (STP), $NH_3 = 500$ ppm, $NOx = 500$ ppm, $H_2O = 8\%$ v/v, $O_2 = 8\%$ v/v. $NO_2/NOx = 0$, 0.25, 0.5, 0.75, 1. (A) NOx conversion (B) NH_3 conversion (C) N_2 selectivity. Symbols = experimental. Solid lines = kinetic fit.

to 0.25, 0.5, 0.75 and 1. Symbols in Fig. 7 represent the measured steady-state NOx conversions (Fig. 7A), NH_3 conversions (Fig. 7B) and N_2-selectivity (Fig. 7C) plotted versus temperature as a function of the NO_2/NOx feed ratio.

It is evident from Fig. 7 that the DeNOx performance of the catalyst is worse for the limiting situations where either NO or NO_2 are the only NOx species present in the reacting system together with NH_3 ($NO_2/NOx = 0$ or 1). Better performances were obtained with NOx feed mixtures containing 25% of either NO or alternatively NO_2, but in the whole temperature range the highest DeNOx activity by far, accompanied also by total NH_3 consumption, was observed when equimolar amounts of NO and NO_2 were fed to the reactor ($NO_2/NOx = 0.5$). This is indeed associated with the activity of the Fast SCR reaction (R.12), which is well known to be extremely active over Fe-zeolites [2,4,36]. Furthermore, the selectivity to N_2 only slightly decreased below 100% when a large excess of NO_2 was present in the feed stream ($NO_2/NOx \geq 0.75$).

The main reactions prevailing in the analyzed reacting systems vary depending on both the NO_2/NOx feed ratio and the temperature [4,36] and are in line with the kinetic scheme reported in the "Reaction network and kinetics" section considering (R.1)–(R.12). A global multiresponse nonlinear regression on the full set of steady state and transient kinetic runs performed over the Fe-zeolite catalyst in the form of powder provided the estimates of the rate parameters for reactions (R.5) to (R.12). The parameters for reactions (R.1)–(R.4) were instead kept constant, being previously independently estimated by the dedicated runs described in the previous paragraph. The estimated activation energy for the Standard SCR reaction (R.5) was in the range of 40–50 kJ/mol, in line with literature reports on Fe-zeolite catalysts [2,9,28,37]. A lower value, in the range of 30–40 kJ/mol was determined for the activation energy of the Fast SCR reaction (R.12). This is higher than what reported in the literature on Fe-zeolites: Devadas et al. [2] reported indeed an apparent activation energy of about 7–8 kJ/mol for the same reaction. However it has to be underlined that this value was estimated using a catalyst in the form of a washcoated monolith, thus mass transfer effects cannot be ruled out. Finally, consistently with the trend of N_2 selectivity in the presence of NO_2 excess, the activation energy of the NO_2-SCR reaction (R.11) (120–140 kJ/mol) was found to be higher than that of the N_2O formation reaction (R.10) (70–80 kJ/mol).

The fit results are compared in Figs. 5–7 (thick lines) with the experimental data. A reasonably good match between experimental data and kinetic fit can be noticed for all the presented runs. In particular, it has to be emphasized that the model nicely reproduced the dynamic features related to the Standard SCR reaction, as indeed, the inhibiting effect of NH_3 on the Standard SCR reaction has been taken into account in the corresponding rate equation (reaction (R.6)). In agreement with the data, the model predicts qualitatively and quantitatively a maximum in the DeNOx activity at both NH_3 feed and shut-off, as apparent from inspection of Fig. 6A (thick lines). In fact, the model was able to reproduce the observed transient NH_3 coverage dependence of the NO conversion with a good quantitative agreement (thick lines in Fig. 6B): it is apparent that the proposed NH_3 inhibition mechanism and the related rate equations, Eqs. (6) and (7), are indeed able to capture the hysteresis effects observed upon NH_3 injection and shut-off.

A second important aspect to be emphasized is the good quality of the steady state kinetic fit in the whole investigated ranges of temperatures and NO_2/NOx feed ratios. From Fig. 7 (solid lines) it is indeed evident that the effect of changing both the feed gas composition and the temperature is well captured by the model in terms of both NOx and NH_3 conversions, as well as in terms of product selectivities.

3.1.4. N_2O reactivity

Fe-zeolites are known to be active both in the catalytic decomposition of N_2O to N_2 [20–22] and in the SCR of N_2O by NH_3 [2,23,24]. Indeed, several papers can be found in the literature regarding mechanistic aspects and kinetic features [2,20–24] of the N_2O catalytic decomposition: it is also well established that, specifically over Fe-zeolites, the presence of NO, or in general of NOx, even in small amounts ("catalytic effect") can significantly enhance the N_2O decomposition rate [21,22]. Nevertheless, to our knowledge, a SCR kinetic model which takes into account also the N_2O decomposition/reactivity over Fe-zeolites cannot be found in the literature so far.

In this context, we performed dedicated steady state kinetic experiments to study the reactivity of N_2O over the tested

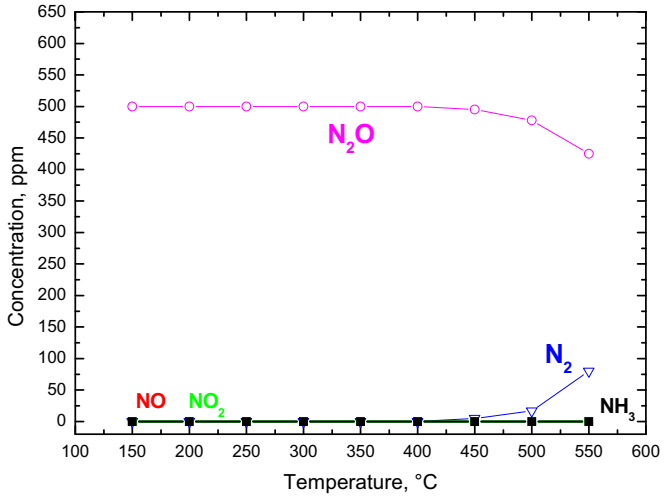

Fig. 8. Decomposition of N_2O as a function of temperature over crushed monolith powder: $Q = 250\,cm^3/min$ (STP), $N_2O = 500$ ppm, $H_2O = 8\%$, $O_2 = 8\%$. Lines and symbols = experimental.

Fe-zeolite catalyst within the overall NH_3-SCR process. First, the N_2O decomposition was investigated at steady state in the 150–550 °C T-range feeding to the reactor 500 ppm of N_2O together with O_2 (8% v/v), H_2O (8% v/v) and balance helium. Results are shown in Fig. 8, in terms of species outlet concentrations versus temperature (lines and symbols). A significant catalytic activity was apparent only above 450–500 °C, where the N_2O decomposition leads to the production of N_2, reaching a maximum conversion of only 15% at the highest investigated temperature of 550 °C. No other nitrogen-containing products were detected.

The effect of NO*x* on the N_2O decomposition reaction was then addressed. The symbols in Fig. 9A show the data collected in the 150–550 °C T-range when feeding 500 ppm of N_2O together with 500 ppm of NO, O_2 (8% v/v), H_2O (8% v/v) and balance helium. In this case N_2O started to be consumed above 350 °C and reaching a maximum conversion of about 55% at 550 °C. Comparing the data presented in Figs. 8 and 9A, it is evident that a significant enhancement of the N_2O decomposition activity occurred in the presence of NO*x*, in line with reports, e.g. by Perez-Ramirez et al. [22] and Kaucký et al. [21] over Fe-zeolites. The "catalytic effect" of NO*x* was confirmed by the fact that the total amount of outlet NO*x* was always equal to the amount of fed NO*x* within experimental error. Furthermore it has to be emphasized that a significant conversion of NO (about 30%), with corresponding production of NO_2, was recorded when N_2O started to be significantly converted. Such a level of NO conversion to NO_2 cannot be ascribed only to the occurrence of the reverse of NO oxidation (R.4), known to be active over Fe-zeolites [4,19,36], but is fully justified by the occurrence of reaction (R.13). The NO_2 concentration levels, e.g. at 550 °C were indeed higher than those calculated according to the thermodynamic equilibrium of reaction (R.4), which is evidence for the occurrence of reaction (R.13), as already reported by other authors [22,25].

When NO_2 was fed to the reactor together with N_2O (Fig. 9B symbols), a slightly different picture was observed: the enhancement of the N_2O decomposition activity was less pronounced, with significant N_2O conversion only above 400–450 °C. Interestingly, the onset of the N_2O decomposition occurred simultaneously with the appearance of noticeable amounts of NO at the reactor outlet, thus consistent with the onset of the NO_2 decomposition reaction (R.4).

Finally, the addition of both NO and NO_2 ($NO_2/NOx = 0.5$) to the reactor feed stream, together with N_2O, resulted again in the

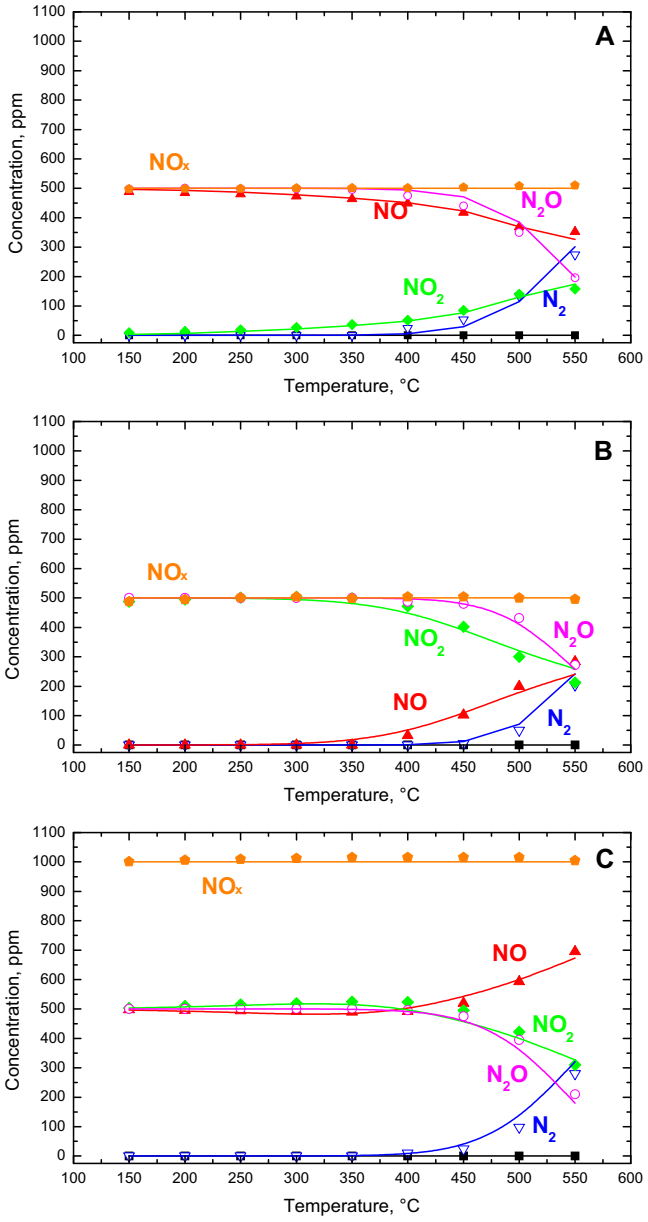

Fig. 9. NO*x* assisted decomposition of N_2O as a function of temperature over crushed monolith powder: $Q = 250\,cm^3/min$ (STP), $N_2O = 500$ ppm; $H_2O = 8\%$ v/v, $O_2 = 8\%$ v/v. (A) NO = 500 ppm (B) $NO_2 = 500$ ppm; (C) $NO = NO_2 = 500$ ppm. Symbols = experimental. Solid lines = kinetic fit.

enhancement of N_2O decomposition (Fig. 9C symbols), with significant activity above 400 °C and significant NO_2 conversion to NO only above 450 °C.

Finally, the reactivity of N_2O with NH_3 was studied in steady state runs. Fig. 10 (symbols) shows the species outlet concentrations versus temperature for a test performed feeding to the test reactor 500 ppm of both N_2O and NH_3 together with O_2 (8% v/v), H_2O (8% v/v) and balance helium. According to Fig. 10, NH_3 started to be converted already at 300 °C with a corresponding N_2 production. At higher temperatures also N_2O started to react, and above 450 °C the consumption of N_2O overcame that of NH_3. Species outlet concentrations in Fig. 10 are consistent with the simultaneous occurrence of the NH_3 oxidation reactions (R.2)–(R.3) and of reaction (R.14), wherein NH_3 reacts selectively with N_2O to form N_2. The contribution of a significant NH_3 oxidation activity, likely responsible for the higher conversion of NH_3 with respect to N_2O, was mainly observed in the intermediate T-region.

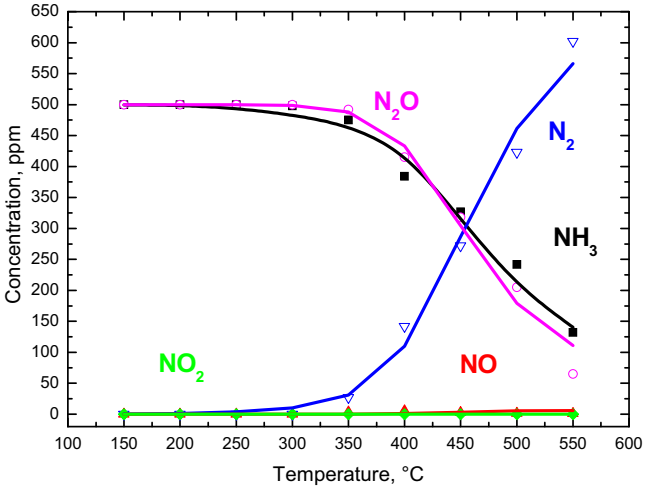

Fig. 10. Reactivity of NH_3–N_2O as a function of temperature over crushed monolith powder: $Q = 250\ cm^3/min$ (STP), $N_2O = 500$ ppm, $NH_3 = 500$ ppm, $H_2O = 8\%$ v/v, $O_2 = 8\%$ v/v. Symbols = experimental. Solid lines = kinetic fit.

In order to take into account the observed N_2O decomposition/reactivity in the kinetic model, reactions (R.13) and (R.14) were included in the developed SCR reaction network. Furthermore, since in real exhausts the presence of N_2O in the absence of NO*x* is an unrealistic option, the direct N_2O decomposition (R.15) was not considered, while the intrinsic rate parameters of the N_2O reduction by NO (R.13) were estimated on the basis of the experimental runs in Fig. 9. Activation energies between 100 and 150 kJ/mol were estimated for both (R.13) and (R.14), again in line with the available literature data on Fe-zeolites [22].

The thick solid lines in Figs. 9 and 10 show the results of the kinetic fit, confirming that the model was able to describe with a good degree of accuracy also the N_2O decomposition/reactivity observed under typical NH_3-SCR conditions. In Fig. 9A both the N_2O and N_2 outlet concentration profiles were indeed well captured in the whole T-range, together with a very good description of the NO oxidation activity. It is really interesting to analyze the results of the kinetic fit in Fig. 9B: indeed, according to our kinetic scheme, the N_2O decomposition can occur only via reaction of N_2O with NO, a species not present at the reactor inlet during the test shown in Fig. 9B. In this case, however, NO was produced via NO_2 decomposition according to reaction (R.4) reverse, whose rate parameters were independently estimated from dedicated NO oxidation/NO_2 decomposition kinetic runs, as already discussed in the section "Steady state NH_3/O_2, NO/O_2, NO_2/O_2 catalytic activity". As a result, a very good quality of the kinetic fit in terms of N_2O, N_2 and NO*x* concentrations was obtained, as also confirmed by inspection of Fig. 9C.

Based on these results it can be stated that the coupling of reactions (R.4) and (R.13) allows a kinetically consistent description of the NO*x* assisted N_2O decomposition in the whole range of NO_2/NO*x* ratios (from 0 to 1). Furthermore, at the same time this scheme allows also the correct representation of the enhanced NO oxidation activity in the presence of N_2O, which can result in a significant change of the NH_3-SCR activity over Fe-zeolite catalytic systems, as extensively discussed in the previous paragraph.

The N_2O consumption was also well reproduced by the model for the NH_3/N_2O reacting system, only a slight underestimation of both N_2O and NH_3 conversions being evident at the highest temperature, namely 550 °C.

3.2. Lab scale experiments: runs over monolith catalyst

The first step of the model scale-up process is described in the following paragraphs: initially, catalytic activity runs were carried out over a small core monolith sample in a lab rig; these data were then used to validate the SCR intrinsic kinetics herein developed by comparison with model simulations generated by incorporating the SCR kinetics into the transient 1D + 1D mathematical model of SCR monolith converters already described in [13,14].

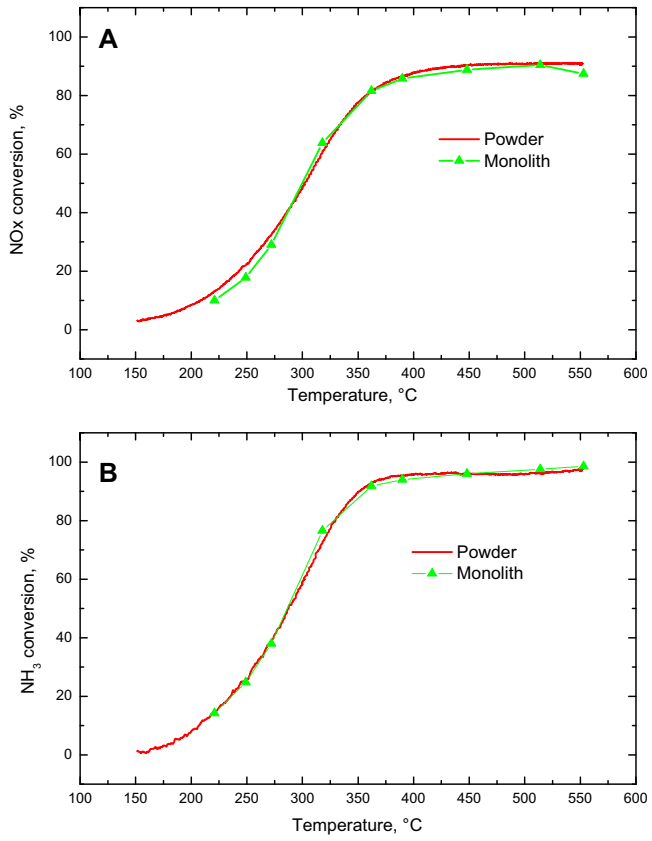

Fig. 11. Reactivity of NH_3–NO as a function of temperature over crushed monolith powder and monolith catalyst: $SV = 681{,}800\ cm^3/h\ g_{active\ phase}$ (STP), NO = 500 ppm, $NH_3 = 500$ ppm, $H_2O = 8\%$ v/v, $O_2 = 8\%$ v/v. (A) NO*x* conversion (B) NH_3 conversion. Red solid line = crushed monolith. Green line + symbols = monolith catalyst. (For interpretation of the references to color in this figure legend, the reader is referred to the web version of the article.)

In the first step of the model scale-up process the importance of mass transfer limitations was evaluated by comparing results obtained at similar operating conditions over the crushed monolith powder and over the core monolith sample. Fig. 11 shows experimental results in terms of NO*x* (Fig. 11A) and NH_3 (Fig. 11B) conversions when a steady state experiment was carried out with a feed stream of 500 ppm NH_3 and NO, O_2 (8% v/v) and H_2O (8% v/v). Inspection of Fig. 11 points out very similar results for the catalyst either in the powdered or in the monolithic form, thus indicating minor mass transfer limitations for the tested monolith catalyst in the investigated range of experimental conditions. Notably, this conclusion should not be generalized, since recent reports have pointed out the appearance of both external and internal (washcoat) diffusion limitations in Cu- and Fe-zeolite SCR monolith catalysts at intermediate – high temperatures [26,27].

3.2.1. Steady state NH_3/NO–NO_2/O_2 catalytic activity

Fig. 12 illustrates the results of steady state experiments performed at different temperatures feeding NH_3 (500 ppm), NO*x* (500 ppm), O_2 (8% v/v), H_2O (8% v/v) and balance N_2 to the core monolith catalyst sample used in lab-scale validation tests; symbols indicate experimental data, solid lines are the model predictions. These runs differ only in the NO_2/NO*x* feed ratios (A: $NO_2/NOx = 0$; B: $NO_2/NOx = 0.5$; C: $NO_2/NOx = 1$) and are thus

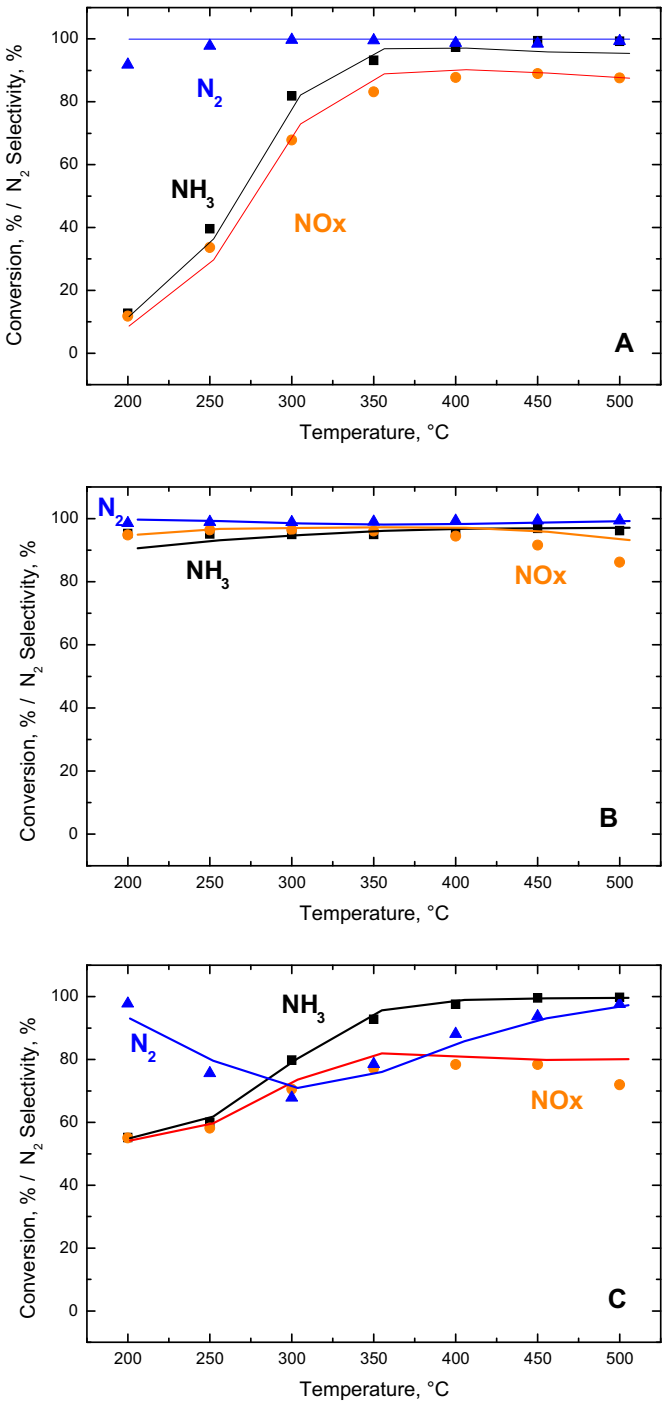

Fig. 12. Reactivity of NH_3–NO–NO_2–O_2 as a function of temperature over the monolith catalyst for different NO_2/NOx feed ratios: GHSV = 100,000 h^{-1}, NH_3 = 500 ppm, NOx = 500 ppm, H_2O = 8% v/v, O_2 = 8% v/v. (A) NO_2/NOx = 0, (B) NO_2/NOx = 0.5, (C) NO_2/NOx = 1. Symbols = experimental. Solid lines = model simulation.

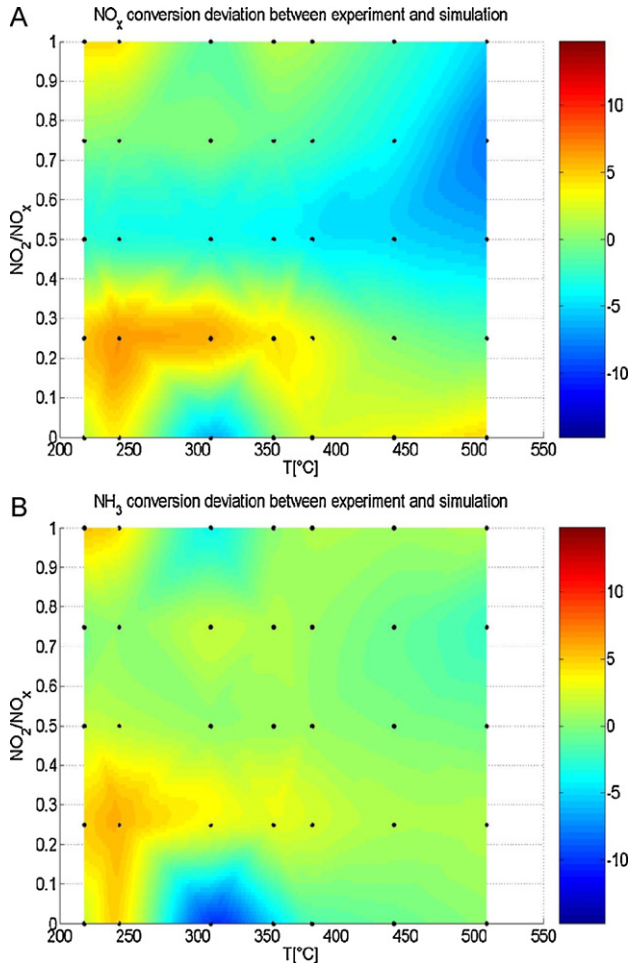

Fig. 13. Absolute NH_3 (A) and NOx (B) conversion deviations between experimental data and model simulation for steady state runs over the monolith catalyst as a function of temperature and NO_2/NOx. GHSV = 100,000 h^{-1}, NH_3 = 500 ppm, NOx = 500 ppm, H_2O = 8% v/v, O_2 = 8% v/v.

representative of the three main SCR reacting systems, namely Standard, Fast and NO_2-SCR.

When only NO was present in the feed stream together with NH_3 (Fig. 12A), the DeNO*x* activity was limited in the low-T region (T < 250 °C); it increased then with growing temperature until reaching total NH_3 conversion at 350–400 °C, in parallel with about 90% NO conversion. When equimolar amounts of NO and NO_2 (Fig. 12B) were fed to the SCR monolith in the presence of NH_3, an extremely high DeNO*x* efficiency was achieved, with almost total conversion of all the reactants already at 200 °C. The high DeNO*x* efficiency was maintained up to 400 °C, while at higher temperatures increasing amounts of NO were detected at the reactor outlet. When NO_2 was the only NO*x* source (Fig. 12C), the low-T DeNO*x* activity was significant, but lower than in the case of NO_2/NOx = 0.5, while at higher temperatures (T > 350 °C) the NO*x* conversion was limited by the stoichiometry of the NO_2-SCR reaction (R.11), as total NH_3 conversion was achieved. Only for this test the selectivity to N_2 was less than 95%, indicating a dependence of the product selectivity on the NO_2/NOx ratio, in line with the results over the powdered monolith (Fig. 7).

For all the presented tests a fairly good match between predictive model simulations and experimental data can be observed in the whole temperature range and for all the NO_2/NOx feed ratios.

In order to produce a full overview of the steady state model validation, experiments were also run and simulated with intermediate NO_2/NOx feed ratios, namely 0.25 and 0.75, and so-called validation maps were created for NO*x* and NH_3 conversions. Such maps show validation results in terms of absolute error between experimental and simulated percentage conversions at steady state conditions. These data are plotted as a function of temperature and NO_2/NOx feed ratio: symbols represent conditions where experimental data have been collected and the relative model error has been evaluated; a visual indication of the model prediction quality is given by associating a colour scale to the error, which is calculated for all the investigated conditions range with interpolation of the available discrete data. Fig. 13 shows that model deviations were

in the range of ±5% for both NH_3 and NO*x* conversions almost in the whole investigated field. The regions where the error is greatest correspond to a NO_2/NO*x* ratio of 0.25 and temperatures between 200 and 250 °C, with errors close to 5%, and NO_2/NO*x* ratio of 0 and temperatures around 300 °C, where a maximum error of about 9.8% was observed for the simulation of NH_3 conversion. This is the only point over the whole range of experimental conditions where the deviation between experiments and simulations at steady state conditions was significantly above 5%, thus no systematic deviation between experiments and predictive simulations can be identified by the analysis of Fig. 13.

3.2.2. Transient experiments

The derived SCR model was further validated by simulating transient runs performed over the small core monoliths. In analogy to the TRM runs over the powdered catalyst, 750 ppm of NH_3 were fed to the core monolith sample in a stepwise manner while continuously flowing NO*x* (500 ppm), O_2 (8% v/v), H_2O (8% v/v) and balance N_2 at a constant temperature in the range 200–350 °C.

Fig. 14 shows the results of one experiment performed at 250 °C by feeding and removing the NH_3 feed flow every 300 s for different NO_2/NO*x* feed ratios, namely 0 (Fig. 14A), 0.25 (Fig. 14B) and 0.5 (Fig. 14C): the figure compares the measured (thin lines) and simulated (thick lines) outlet concentration profiles of NH_3, NO and NO_2 during such tests.

It can be noticed that when NO was the only NO*x* species in the system (Fig. 14A), a maximum in the DeNO*x* activity at both NH_3 injection and shut-off characterized the system dynamics, as already observed over the catalyst in the powdered form (see Fig. 6). Such a dynamic behaviour is attributed to the inhibiting effect of NH_3 on the Standard SCR reaction and, as apparent from Fig. 14A, the model of themonolithic SCR converter can reproduce it quantitatively.

The addition of NO_2 to the reactor feed dramatically changed both the system dynamics and the activity. Indeed, when NO*x* consisted of 25% NO_2 (Fig. 14B), a clear maximum in the DeNO*x* activity was still present at NH_3 feed, but on the opposite it was no more observed at NH_3 shut-off. Notably, the simulation shows the same qualitative behaviour, though a slight overestimation of the DeNO*x* activity at NH_3 shut-off is evident. The further increment of NO_2 up to 50% (Fig. 14C) strongly enhanced the DeNO*x* activity, leading to total NO*x* conversion and very fast dynamics, as correctly predicted by the model. Thus, a good quantitative agreement between data and simulation was observed for all the dynamic runs, except for some deviations in the test with a NO_2/NO*x* feed ratio of 0.25.

3.2.3. N_2O reactivity

Figs. 15 and 16 show validation results for two T-ramp experiments over the monolith catalyst involving N_2O decomposition/reactivity.

In Fig. 15, NH_3 and N_2O (200 ppm each) were fed to the reactor in a stepwise manner at about $t = 4025$ s and $t = 5400$ s, respectively, while continuously flowing H_2O (8% v/v) and O_2 (8% v/v) in a N_2 stream at a constant temperature of 150 °C. Then, at about $t = 6600$ s, the temperature started being increased with an average rate of about 11 °C/min up to 540 °C. Thin lines represent the measured species outlet concentrations as a function of time: as soon as added to the feed stream, outlet N_2O reached its feed concentration, indicating that such a species was neither reactive at this low temperature nor significantly adsorbed on the catalyst. Then, upon increasing the temperature, N_2O started to be reduced by NH_3 according to reaction (R.14), reaching about 43% conversion at high temperature. Contrary to N_2O, the NH_3 trace showed a significant dead time (about 90 s) related to the adsorption of NH_3 on the catalyst surface. When the temperature started to be increased, first desorption of the previously adsorbed NH_3 occurred (the outlet

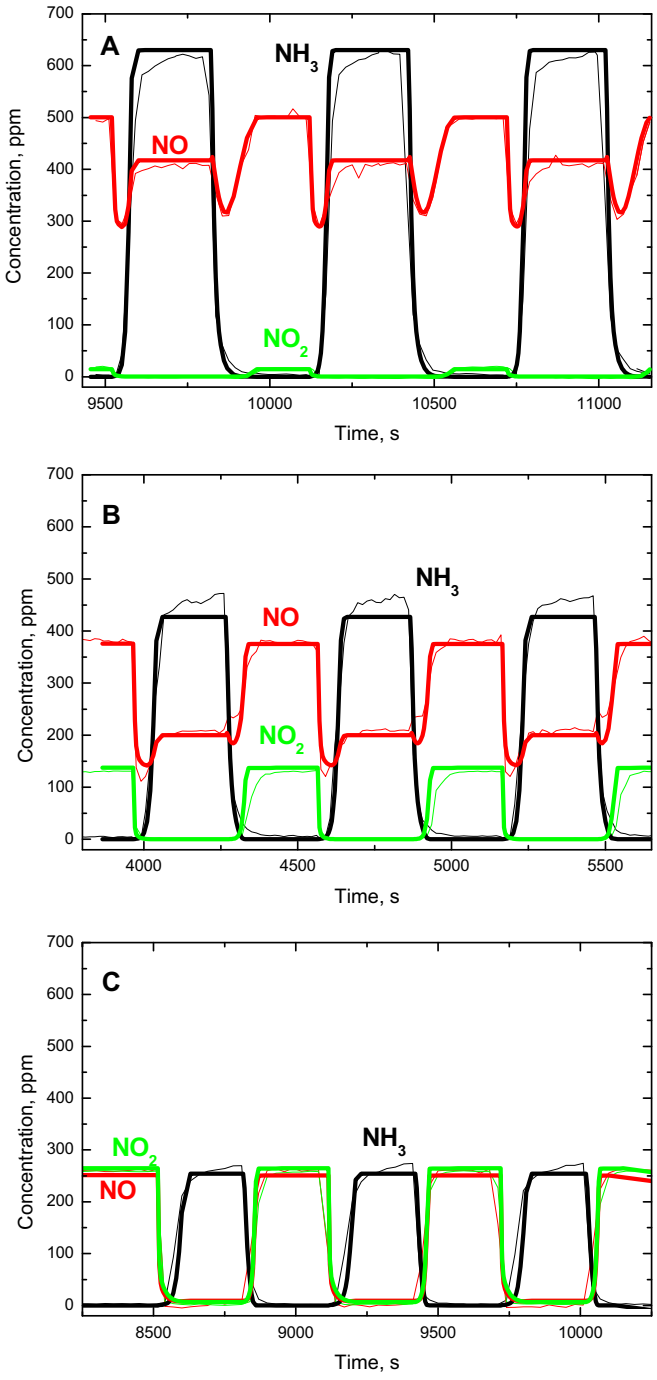

Fig. 14. Concentration step change experiments for the NH_3–NO–NO_2–O_2 reacting system over the monolith catalyst: $T = 250$ °C, GHSV = 100,000 h^{-1}, NH_3 = 500 ppm, NO*x* = 500 ppm, H_2O = 8% v/v, O_2 = 8% v/v. NH_3 pulse length = 300 s. (A) NO_2/NO*x* = 0 (B) NO_2/NO*x* = 0.5 (C) NO_2/NO*x* = 1. Thin lines = experimental. Thick lines = model simulation.

concentration was in fact higher than the feed one), then, in parallel with the onset of N_2O reduction, the NH_3 signal started to drop, leading to a conversion of NH_3 of about 38% at 540 °C.

After a modest adjustment of the rate parameters of the NH_3 oxidation only in order to account for a slight change of catalyst activity with time-on-stream, simulation results (thick lines) were in fairly good agreement with both the N_2O and the NH_3 concentration traces.

A similar experiment was then repeated after changing the feed composition. In Fig. 16, 200 ppm of N_2O were stepwise fed to the

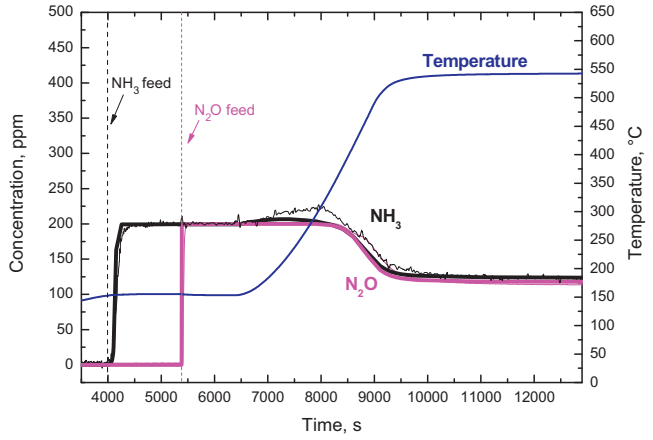

Fig. 15. Reactivity of NH_3–N_2O during TPR over the monolith catalyst: GHSV = 100,000 h^{-1}, N_2O = 200 ppm, NH_3 = 200 ppm, H_2O = 8% v/v, O_2 = 8% v/v, T-ramp ≈11 °C/min. Thin lines = experimental. Thick lines = model simulations.

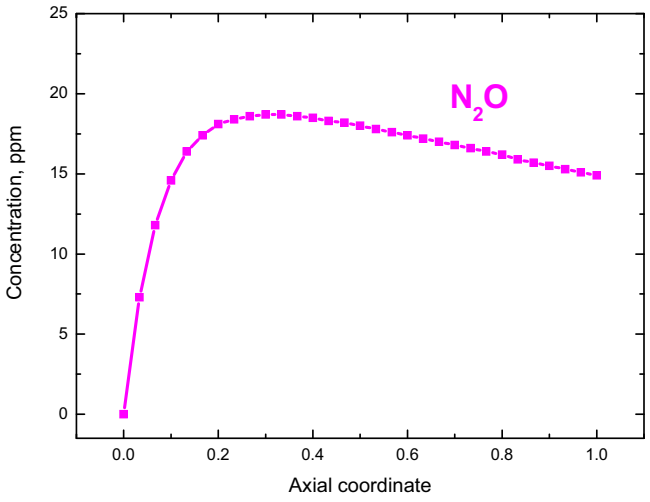

Fig. 17. Simulated N_2O concentration profile along the monolith dimensionless axial coordinate at steady state conditions: T = 500 °C, GHSV = 28,000 h^{-1}. Feed concentrations: NH_3 = 600 ppm, NO_2 = 600 ppm, H_2O = 8% v/v, O_2 = 8% v/v.

reactor at t = 4700 s, followed by the feed of 200 ppm of NO at t = 4200 s. The gaseous feed stream included also H_2O (8% v/v), O_2 (8% v/v) and balance N_2, but no ammonia. The temperature was first kept constant at about 150 °C, then a temperature ramp at about 11 °C/min was performed until 540 °C, while continuously feeding the reacting mixture. During this test (thin lines in Fig. 16), and in line with the results in Fig. 15, N_2O reached instantaneously a steady state concentration equal to the feed value, indicating negligible adsorption and reactivity of this species at 150 °C. On increasing the temperature, the N_2O outlet concentration monotonically decreased, this time because of the N_2O reduction by NO, reaction (R.13), eventually reaching 35% conversion at 540 °C. Furthermore also a significant NO conversion to NO_2 was observed when increasing the temperature, reaching 25% at 540 °C.

These data were then successfully compared with purely predictive model simulations (thick lines), highlighting a very good simulation quality over the whole test and for all the measured species.

3.2.4. Role of N_2O reactivity in the NO_2 SCR reaction

As a final step, the validated kinetic model was applied to investigate the importance of the N_2O reactions in the NH_3/NO_2 reacting system. As discussed in previous paragraphs, the NO_2-SCR (R.11) is the main reaction occurring with this feed composition within typical SCR temperature ranges, namely above 250 °C. However, the mechanism of this reaction is still debated in the literature. On the basis of transient reactivity experiments [38] some of us recently proposed a key role of surface nitrates as intermediates in the NO_2-SCR reaction mechanism: the NO_2-SCR activity would result in fact from the formation of nitrates via NO_2 disproportionation, followed by their selective reduction by NH_3, being this last step rate determining and likely associated with a red-ox process wherein NH_3 directly reduces the catalyst sites, which are then reoxidized by surface nitrates.

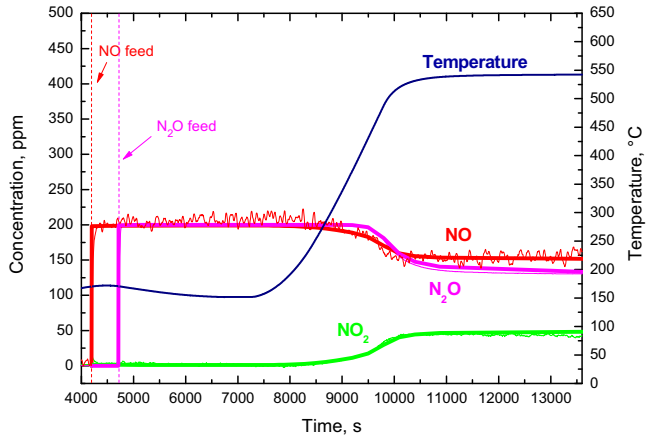

Fig. 16. NO assisted decomposition of N_2O during TPR over the monolith catalyst: GHSV = 100,000 h^{-1}, N_2O = 200 ppm, NO = 200 ppm, H_2O = 8% v/v, O_2 = 8% v/v, T-ramp ≈11 °C/min. Thin lines = experimental. Thick lines = model simulations.

On the other hand it has been recently proposed by Iwasaki and Shinjoh [39] that the NO_2-SCR reaction (R.11) might progress sequentially via N_2O formation, according to reaction (R.10), and subsequent reduction of N_2O by NH_3 according to reaction (R.14). The sum of these two reactions results indeed in the stoichiometry of the NO_2-SCR reaction (R.11). Furthermore, Luo et al. [40] have recently proved, by means of spatially resolved gas concentration analysis, that at high temperatures N_2O is formed in the front part of an SCR monolith, while it is consumed in the rear part of it. However this phenomenon was recorded by the authors only at temperatures higher than 400 °C.

During the development of the kinetic model presented in this paper, an independent estimate of the catalyst activity in N_2O reduction/decomposition was provided by the dedicated tests illustrated in Figs. 9 and 10. From these tests it can be emphasized that the threshold temperature for the onset of N_2O reduction by NH_3 was between 350 °C and 400 °C in our runs. On the opposite, the increase of N_2 selectivity for the NH_3/NO_2 reacting system (Fig. 7C), signaling the onset of the NO_2-SCR reaction (R.11), started at 275 °C, thus pointing to a much lower threshold temperature (−75 °C) for the NO_2-SCR reaction.

In addition to this direct experimental evidence it is worth mentioning that in an early stage of model development we did not include the NO_2-SCR reaction (R.11) in the kinetic scheme, and we attempted to describe the NO_2-SCR reactivity on the basis of reactions (R.10) and (R.14) only, in line with a sequential scheme where the NO_2-SCR reaction occurs via N_2O formation and its subsequent reduction by NH_3, as also proposed in the literature [39,41]. Preliminary fit results showed that such a scheme was inconsistent, being kinetically limited by the N_2O reduction by NH_3 and therefore underestimating the overall activity. This justified the introduction of an independent NO_2-SCR reaction (R.11), as in the present kinetic scheme.

The potential contribution of N_2O reduction/decomposition in the reactivity of NH_3 and NO_2 was however investigated. For this purpose, Fig. 17 shows the simulated steady-state axial profile of N_2O concentration obtained at 550 °C while feeding to the monolith 500 ppm of NH_3, 500 ppm of NO_2 together with 8% v/v O_2 and 8% v/v H_2O. From inspection of Fig. 17 it can be noticed that the model predicted an increasing N_2O concentration in the front part of the monolith, while the concentration of the same species slowly decreased in the rear part of it, due to N_2O reduction/decomposition. These simulation results are in excellent agreement with the experimental findings of Luo et al. [40], indicating a small but significant contribution of N_2O reduction/decomposition to the NH_3/NO_2 SCR reacting system at high temperatures, namely above 350 °C.

4. Conclusions

We have herein presented a systematic investigation of the $NO/NO_2/N_2O–NH_3$ SCR reactions over a commercial Fe-zeolite catalyst, tested both as a powdered sample and in its original shape of a washcoated honeycomb monolith catalyst, in view of modelling SCR catalytic converters for diesel vehicles. The kinetic study discussed in Section 3.1 covers the full range of possible NO_2/NOx feed ratios (0–1) in the relevant temperature window (150–550 °C).

In the presence of NO as the only NOx source the Standard SCR reaction was found to be the dominant reaction, with a slight contribution of NH_3 oxidation prevailing only at high temperatures. For the same reacting system the analysis of transient NH_3 supply pointed out a strong inhibition of this species on the Standard SCR reaction at temperatures below 300 °C, which resulted in an enhanced DeNOx activity at both NH_3 opening and shut-off.

The situation changed when also NO_2 was added to the feed stream: the prevailing reactions in the analyzed reacting systems vary in this case depending on both the NO_2/NOx feed ratio and the temperature. In any case the DeNOx performance was worse for the limiting situations where either NO or NO_2 were the only NOx species in the feed stream together with NH_3. In the whole temperature range the highest DeNOx activity was observed when equimolar amounts of NO and NO_2 were fed to the reactor, due to the occurrence of the Fast SCR reaction. N_2 was the main product in the entire range of experimental conditions investigated, the N_2 selectivity falling slightly below 100% only when a large excess of NO_2 was present in the feed stream ($NO_2/NOx \geq 0.75$).

Besides the Standard-SCR, Fast-SCR and NO_2-SCR reactions, the present kinetic study addressed also the reactivity of N_2O in relation to its NO-assisted decomposition and to its selective catalytic reduction with NH_3. Both reactions were found to be active above 350 °C and 100% selective to N_2. Furthermore our data evidenced an enhanced NO oxidation activity in the presence of N_2O, thus emphasizing an interplay between the N_2O reactivity and the NH_3-SCR reactions, the latter ones being dramatically influenced by the NO_2/NOx ratio, as extensively reported in the paper and widely recognized in the literature on Fe-zeolite SCR catalysts.

A global kinetic model was developed in order to fully describe the $NO/NO_2/N_2O–NH_3$ SCR reacting system, thus also including account both of the SCR reactivity in presence of a strong excess of NO_2 and of the N_2O reactivity. Furthermore, experiments over the catalyst in its two tested configurations (powders vs. honeycomb) reported in Sections 3.1 and 3.2 showed that the developed simulation model can adequately account for the impact of external and intraporous mass transfer resistances onto both steady-state and transient performances of SCR converters: such an impact was however very limited at the conditions of the present study. While a number of SCR kinetic studies and models have recently appeared in the literature, none of them to our knowledge incorporates simultaneously all of these features, each one of them being however critical for realistic simulation of SCR units in aftertreatment systems.

References

[1] T.V. Johnson, SAE Technical Paper 2011-01-0304.
[2] M. Devadas, O. Kröcher, M. Elsener, A. Wokaun, N. Söger, M. Pfeifer, Y. Demel, L. Mussmann, Applied Catalysis B: Environmental 67 (2006) 187–196.
[3] P. Forzatti, L. Lietti, E. Tronconi, Nitrogen Oxides Removal—Industrial, John Wiley & Sons, Inc., New York, 2002.
[4] A. Grossale, I. Nova, E. Tronconi, Catalysis Today 136 (2008) 18–27.
[5] M. Koebel, G. Madia, M. Elsener, Catalysis Today 73 (2002) 239–247.
[6] H. Sjövall, L. Olsson, E. Fridell, R.J. Blint, Applied Catalysis B: Environmental 64 (2006) 180–188.
[7] S. Brandenberger, O. Kroecher, A. Tissler, R. Althoff, Catalysis Reviews: Science and Engineering 50 (2008) 492–531.
[8] C. Ciardelli, I. Nova, E. Tronconi, D. Chatterjee, B. Bandl-Konrad, M. Weibel, B. Krutzsch, Applied Catalysis B: Environmental 70 (2007) 80–90.
[9] M. Iwasaki, K. Yamazaki, H. Shinjoh, Applied Catalysis A: General 366 (2009) 84–92.
[10] M. Koebel, M. Elsener, M. Kleemann, Catalysis Today 59 (2000) 335–345.
[11] K. Rahkamaa-Tolonen, T. Maunula, M. Lomma, M. Huuhtanen, R.L. Keiski, Catalysis Today 100 (2005) 217–222.
[12] D. Chatterjee, T. Burkhardt, M. Weibel, I. Nova, A. Grossale, E. Tronconi, SAE Technical Paper 2007-01-1136.
[13] D. Chatterjee, T. Burkhardt, M. Weibel, E. Tronconi, I. Nova, C. Ciardelli, SAE Technical Paper 2006-01-0468.
[14] E. Tronconi, I. Nova, C. Ciardelli, D. Chatterjee, B. Bandl-Konrad, T. Burkhardt, Catalysis Today 105 (2005) 529–536.
[15] C. Ciardelli, I. Nova, E. Tronconi, B. Konrad, D. Chatterjee, K. Ecke, M. Weibel, Chemical Engineering Science 59 (2004) 5301–5309.
[16] I. Nova, C. Ciardelli, E. Tronconi, D. Chatterjee, B. Bandl-Konrad, AIChE Journal 52 (2006) 3222–3233.
[17] I. Nova, C. Ciardelli, E. Tronconi, D. Chatterjee, M. Weibel, AIChE Journal 55 (2009) 1514–1529.
[18] L. Lietti, I. Nova, S. Camurri, E. Tronconi, P. Forzatti, AIChE Journal 43 (1997) 2559–2570.
[19] H. Sjövall, R.J. Blint, A. Gopinath, L. Olsson, Industrial & Engineering Chemistry Research 49 (2010) 39–52.
[20] A. Guzmán-Vargas, G. Delahay, B. Coq, Applied Catalysis B: Environmental 42 (2003) 369–379.
[21] D. Kaucký, Z. Sobalík, M. Schwarze, A. Vondrová, B. Wichterlová, Journal of Catalysis 238 (2006) 293–300.
[22] J. Pérez-Ramírez, F. Kapteijn, G. Mul, J.A. Moulijn, Journal of Catalysis 208 (2002) 211–223.
[23] B. Coq, M. Mauvezin, G. Delahay, J.-B. Butet, S. Kieger, Applied Catalysis B: Environmental 27 (2000) 193–198.
[24] B. Coq, M. Mauvezin, G. Delahay, S. Kieger, Journal of Catalysis 195 (2000) 298–303.
[25] F. Kapteijn, G. Marbán, J. Rodriguez-Mirasol, J.A. Moulijn, Journal of Catalysis 167 (1997) 256–265.
[26] J.W. Beeckman, Industrial & Engineering Chemistry Research 30 (1991) 428–430.
[27] R.S. Cunningham, C.J. Geankoplis, Industrial & Engineering Chemistry Fundamentals 7 (1968) 535–542.
[28] P.S. Metkar, N. Salazar, R. Muncrief, V. Balakotaiah, M.P. Harold, Applied Catalysis B: Environmental 104 (2011) 110–126.
[29] L. Rodríguez-González, F. Hermes, M. Bertmer, E. Rodríguez-Castellón, A. Jiménez-López, U. Simon, Applied Catalysis A: General 328 (2007) 174–182.
[30] K. Kamasamudram, N.W. Currier, X. Chen, A. Yezerets, Catalysis Today 151 (2010) 212–222.
[31] A. Schuler, M. Votsmeier, P. Kiwic, J. Gieshoff, W. Hautpmann, A. Drochner, H. Vogel, Chemical Engineering Journal 154 (2009) 333–340.
[32] S. Malmberg, M. Votsmeier, J. Gieshoff, N. Soger, L. Mussmann, A. Schuler, A. Drochner, Topics in Catalysis 42–43 (2007) 33–36.
[33] S.A. Stevenson, J.C. Vartuli, C.F. Brooks, Journal of Catalysis 190 (2000) 228–239.
[34] M. Wallin, C.-J. Karlsson, M. Skoglundh, A. Palmqvist, Journal of Catalysis 218 (2003) 354–364.
[35] Z. Sobalik, K. Jisa, H. Jirglova, B. Bemauer, Catalysis Today 126 (2007) 73–80.
[36] M. Colombo, I. Nova, E. Tronconi, Catalysis Today 151 (2010) 223–230.
[37] H.Y. Huang, R.Q. Long, R.T. Yang, Applied Catalysis A: General 235 (2002) 241–251.
[38] A. Grossale, I. Nova, E. Tronconi, Journal of Catalysis 265 (2009) 141–147.
[39] M. Iwasaki, H. Shinjoh, Applied Catalysis A: General 390 (2011) 71–77.
[40] J.-Y. Luo, X. Hou, P. Wijayakoon, S.J. Schmieg, W. Li, W.S. Epling, Applied Catalysis B: Environmental 102 (2011) 110–119.
[41] P. Markatou, J. Dai, A. Johansson, W. Klink, M. Castagnola, T.C. Watling, M. Tutuianu, SAE Technical Paper 2011-01-1304.